

Photon emission in strong fields beyond the locally-constant field approximation

I. A. Aleksandrov¹, G. Plunien², and V. M. Shabaev¹

¹ *Department of Physics, Saint Petersburg State University,*

7/9 Universitetskaya Naberezhnaya, Saint Petersburg 199034, Russia

² *Institut für Theoretische Physik, TU Dresden, Mommsenstrasse 13, Dresden D-01062, Germany*

We investigate a fundamental nonlinear process of vacuum photon emission in the presence of strong electromagnetic fields going beyond the locally-constant field approximation (LCFA), i.e., providing the exact treatment of the spatio-temporal inhomogeneities of the external field. We examine a standing electromagnetic wave formed by high-intensity laser pulses and benchmark the approximate predictions against the results obtained by means of a precise approach evaluating both the tadpole (reducible) and vertex (irreducible) contributions. It is demonstrated that the previously-used approximate methods may fail to properly describe the quantitative characteristics of each of the two terms. In the case of the tadpole contribution, the LCFA considerably underestimates the number of photons emitted for sufficiently high frequency of the external field. The vertex term predicts emission of a great number of soft photons whose spectrum is no longer isotropic in contrast to the LCFA results. A notable difference among the photon yields along different spatial directions, which is not captured by the LCFA, represents an important signature for experimental studies of the photon emission process. Since this feature takes place unless the Keldysh parameter is much larger than unity, it can also be used in indirect observation of the Schwinger mechanism.

Introduction.—It is well known that Maxwell’s Lagrangian for electrodynamics leads to an inherently linear theory, and the corresponding superposition principle does not allow one solution of Maxwell’s equations to interact with another, i.e., a combination of two classical light waves does not give rise to any additional radiation. However, *quantum* electrodynamics (QED) predicts a phenomenon of photon emission due to quantum fluctuations in the presence of strong external backgrounds [1–4]. This process is closely related to the photon-photon scattering via fermionic loops [1, 5], but one assumes here that the initial state contains no photons while the quantized electron-positron field interacts with a classical external background and the quantized part of the electromagnetic field whose quanta are being emitted.

Although this phenomenon was predicted several decades ago, it has never been investigated experimentally. Nevertheless, a rapid development of the laser technologies significantly stimulates further attempts at finding most favorable scenarios for practical observations of the effect. From the theoretical viewpoint, it requires new accurate and efficient methods be designed. In particular, the presence of the temporal and spatial inhomogeneities of the external fields in experimental setups demands sophisticated techniques in order

to provide adequate predictions for realistic field configurations. In a recent series of studies [6–9], the authors proposed a very productive computational approach based on the so-called locally-constant field approximation (LCFA) which locally treats the external field as a static and spatially uniform background and invokes the closed-form expression for the Heisenberg-Euler effective action [2, 4] (it was also utilized in Refs. [10–13]). Within this approach, one employs an effective interaction operator defined in the Fock space of the photon states and incorporating the one-loop corrections (see, e.g., Ref. [14]). Since this operator does not involve fermionic degrees of freedom, the final expressions turn out to be much less complicated than the exact formulas in terms of the one-particle solutions of the Dirac equation [15]. The LCFA approach allows one to efficiently evaluate the tadpole (reducible) contribution [see Fig. 1(a)] to the spectra of signal photons taking into account the spatio-temporal dependence of complex field configurations. However, the validity of the LCFA in context of various processes is always limited. For instance, the LCFA may fail to properly describe the photon spectra in studies of nonlinear Compton scattering [16–18]. We also point out that according to recent results of precise calculations [19–26], the spatio-temporal inhomogeneities may also play a prominent role in the process of electron-positron pair production. In this Letter, we perform exact calculations going beyond the LCFA to examine its validity.

Furthermore, it turns out that there exists also another contribution besides the tadpole one [see Fig. 1(b)], which appears in the same order of perturbation theory (PT) with respect to the radiative interaction (the photon number density $\sim \alpha$). We will refer to this term as the vertex contribution (alternatively, the irreducible contribution [14]). To our knowledge, it was calculated only in Ref. [27] in the case of a spatially uniform time-dependent electric field. According to Ref. [27], the vertex diagram predicts production of a huge amount of soft photons, which also opens up a possibility for studying nonlinear effects of strong-field QED in

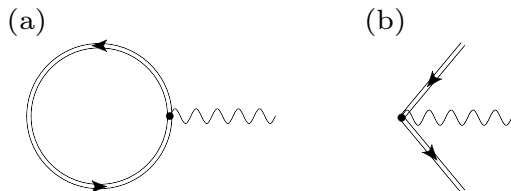


Figure 1. Nonperturbative tadpole (a) and vertex (b) diagrams describing two independent channels of photon emission in a strong external field and giving rise to nontrivial photon number density to first order in the fine-structure constant $\alpha = e^2/(4\pi)$. The double line represents the exact propagator (or solution) in the presence of the external field.

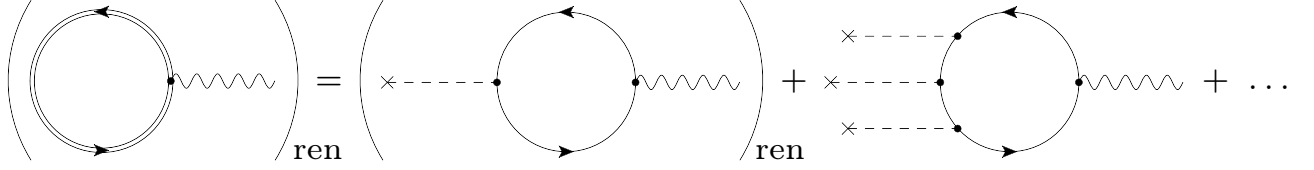


Figure 2. PT expansion of the renormalized tadpole diagram. The dashed lines with crosses denote the interaction with the external field. The renormalized diagram with two external legs does not contribute (see the main text). The diagrams with an odd number of external legs do not appear due to Furry's theorem.

experiments in the not-so-distant future. Note that the vertex diagram describes the photon-emission process accompanying creation of e^+e^- pairs, so experimental measurements of the photon spectra could also allow one to indirectly investigate the Schwinger mechanism of pair production. Since real setups involve external backgrounds depending not only on time but also on the spatial coordinates, it is strongly desirable to examine fields having multidimensional inhomogeneities. Moreover, if the external field depends solely on time, the photons associated with this field carry energy but do not transfer momentum, which could misrepresent the spectra of photons emitted.

Basic expressions.—In the present study, we evaluate the both contributions considering a standing electromagnetic wave with peak electric-field strength E_0 and frequency ω . The vector potential is chosen in the following form (hereafter we use the units $\hbar = c = 1$):

$$A_x(t, z) = \frac{E_0}{\omega} F(t) \sin \omega t \cos \omega z, \quad (1)$$

where $F(t)$ is a smooth envelope function which vanishes unless $t_{\text{in}} \leq t \leq t_{\text{out}}$. The other components of A^μ equal zero. We always choose a large number of cycles ($N \gg 1$). The field configuration chosen has several important advantages. First, this background can be viewed as an approximation for the resulting field of two laser pulses propagating along and opposite the z direction, respectively, and polarized along the x axis [the photons carry momentum $\pm \mathbf{K}$, where $\mathbf{K} = (0, 0, \omega)$]. Although this field configuration is infinite in space and does not depend on x and y , it is a reasonable approximation for a combination of two counterpropagating laser pulses since $N \gg 1$ and Eq. (1) takes into account the spatio-temporal dependence of the carrier neglecting only slowly varying spatial parts pertaining to the envelope. Second, as $N \gg 1$, the external field frequency related to the temporal oscillations is well defined and coincides with that regarding the spatial dependence in accordance with Maxwell's equations. Finally, the spatial periodicity of the external field allows us to efficiently solve the Dirac equation in the momentum representation, which is necessary for evaluating the number density of signal photons within our approach (see below).

The general expressions for the two contributions to the photon number density $n_{\mathbf{k}, \lambda} = dN_{\mathbf{k}, \lambda}/d\mathbf{k}$ [to first order in

$\alpha = e^2/(4\pi)$] read [15, 28]

$$n_{\mathbf{k}, \lambda}^{(\text{tadpole})} = \left| \int d^4x j_{\text{in}}^\mu(x) f_{\mathbf{k}, \lambda, \mu}^*(x) \right|^2, \quad (2)$$

$$n_{\mathbf{k}, \lambda}^{(\text{vertex})} = e^2 \sum_{n, m} \left| \int d^4x +\bar{\varphi}_n(x) \gamma^\mu f_{\mathbf{k}, \lambda, \mu}^*(x) - \varphi_m(x) \right|^2 \quad (3)$$

where $x = (t, \mathbf{x})$, e is the electron charge ($e < 0$), $j_{\text{in}}^\mu(x)$ is the *in*-vacuum expectation value of the current operator, $j_{\text{in}}^\mu(x) \equiv \langle 0, \text{in} | j^\mu(x) | 0, \text{in} \rangle$ [15], $\pm \varphi_n(x)$ are the *in* solutions of the Dirac equation relating to positive (negative) values of energy at the initial time instant $t = t_{\text{in}}$ (m and n incorporate momentum and spin), and $f_{\mathbf{k}, \lambda, \mu}(x) = (2\pi)^{-3/2} (2k^0)^{-1/2} e^{-ikx} \varepsilon_\mu(\mathbf{k}, \lambda)$ is the photon wave function corresponding to momentum \mathbf{k} ($k^0 = |\mathbf{k}|$) and polarization λ of the signal photon. The expression (3) for the vertex contribution in the case of a spatially uniform field can also be found in Ref. [27]. Although this term can be evaluated directly by means of Eq. (3), the tadpole diagram requires renormalization. In Fig. 2 we display its PT expansion where it is indicated that one should renormalize the term with one interaction vertex, which possesses a quadratical divergence. However, it turns out that it does not contribute if proper renormalization of the electron charge is performed. We note indeed that the amplitude contains the renormalized polarization tensor $\Pi^{\mu\nu}(k) \sim (k^\mu k^\nu - k^2 g^{\mu\nu})$, where $k^2 = 0$ since the signal photon is real. The term with $k^\mu k^\nu$ also vanishes because it is contracted with the photon polarization function, $k^\mu \varepsilon_\mu(\mathbf{k}, \lambda) = 0$. Accordingly, the leading contribution is determined by the diagram with four external legs, which can be approximately calculated within the LCFA approach developed in Refs. [6–9]. The leading term is proportional to $(E_0/E_c)^3$, where E_c is the Schwinger critical value [$E_c = m^2 c^3 / (|e| \hbar) = 1.3 \times 10^{16}$ V/cm, where m is the electron mass], while the full tadpole diagram displayed in Fig. 1(a) includes also the higher-order terms $\sim (E_0/E_c)^5$, $(E_0/E_c)^7$ etc. Since the condition $(E_0/E_c)^2 \ll 1$ seems completely realistic, there is no need to evaluate the higher-order terms.

Taking into account the periodicity of the external field (1), one can represent the *in* one-particle solutions of the Dirac equation in the following form (see, e.g., Refs. [29, 30]):

$$\zeta \varphi_{\mathbf{p}, s}(x) = (2\pi)^{-3/2} e^{i\zeta \mathbf{p} \mathbf{x}} \sum_{j=-\infty}^{+\infty} \zeta u_{\mathbf{p}, s}^j(t) e^{i\zeta \omega j z}, \quad (4)$$

where $\zeta = \pm$ and the time-dependent functions $\zeta w_{\mathbf{p},s}^j(t)$ are determined by their asymptotic behavior for $t \leq t_{\text{in}}$. One can then demonstrate that the photon number density has the following form [28]

$$\frac{(2\pi)^3}{V} n_{\mathbf{k},\lambda}^{(\text{tadpole})} = \frac{e^2}{(2\pi)^3} \sum_l \delta(\mathbf{k} - l\mathbf{K}) |\mathcal{A}_{l,\lambda}|^2, \quad (5)$$

where V is the volume of the system and $\mathcal{A}_{l,\lambda}$ are the amplitudes which can, in principle, be calculated to all orders in E_0/E_c . The delta-function in Eq. (5) reflects the momentum conservation law and indicates that the signal photon can be produced after absorbing an integer number of the external-field photons. The energy conservation law does not appear explicitly as we cannot analytically carry out integration over temporal variables. Our calculations revealed that the signal photon is always polarized along the x axis ($\lambda = x$). Moreover, the photon yield is substantially suppressed once $l \neq 1$ as the higher-order harmonics appear only in the higher-order

terms of PT with respect to $(E_0/E_c)^2$ [11, 12]. These points are also predicted by the LCFA, which results in the following expression for the leading-order contribution to the photon number density in terms of the function $\mathcal{A}_{l,\lambda}$ for $l = 1$ and $\lambda = x$:

$$\mathcal{A}_{l=1,x}^{(\text{LCFA})} = \frac{\pi}{180} \frac{(eE_0)^3}{m^6} m^2 \sqrt{2k^0} \int dt e^{-ik^0 t} \times \left(3iQ^3 - Q^2 \frac{\dot{Q}}{\omega} - iQ \frac{\dot{Q}^2}{\omega^2} + 3 \frac{\dot{Q}^3}{\omega^3} \right), \quad (6)$$

where $k^0 = |\mathbf{k}| = \omega$ and $Q(t) \equiv F(t) \sin \omega t$. To simplify the computations, we consider an infinite laser pulse [$F(t) = 1$, $t_{\text{in/out}} \rightarrow \mp\infty$], so the exact result for the leading-order term reads

$$\mathcal{A}_{l=1,x}^{(\text{exact})} = 2\pi \delta(k^0 - \omega) \mathcal{I}^{(\text{exact})}, \quad (7)$$

where

$$\mathcal{I}^{(\text{exact})} = \frac{1}{128} \frac{(eE_0)^3}{m^6} \frac{m^4}{\omega^4} m^2 \sqrt{2\omega} \sum_{\eta_i, \xi_i} \int \frac{d\tilde{\omega}}{2\pi} \int d\mathbf{p} \varepsilon_\mu^*(\mathbf{K}, x) \times \text{Tr}[\gamma^\mu S(\tilde{\omega}, \mathbf{p}) \gamma^1 S(\tilde{\omega} - \xi_1 \omega, \mathbf{p} - \eta_1 \mathbf{K}) \gamma^1 S(\tilde{\omega} - (\xi_1 + \xi_2) \omega, \mathbf{p} - (\eta_1 + \eta_2) \mathbf{K}) \gamma^1 S(\tilde{\omega} - \omega, \mathbf{p} - \mathbf{K})], \quad (8)$$

$S(\tilde{\omega}, \mathbf{p}) \equiv (\tilde{\omega} \gamma^0 - \boldsymbol{\gamma} \mathbf{p} + m)/(m^2 + \mathbf{p}^2 - \tilde{\omega}^2)$ is the electron propagator, and the summations run over $\eta_i, \xi_i = \pm 1$ ($i = 1, 2, 3$) satisfying $\sum \eta_i = \sum \xi_i = 1$. The LCFA prediction (6) takes the form

$$\mathcal{I}^{(\text{LCFA})} = \frac{\pi}{90} \frac{(eE_0)^3}{m^6} m^2 \sqrt{2\omega}, \quad (9)$$

which is to be directly compared with Eq. (8). We also point out that as $l = 1$ and $\lambda = x$, the photons emitted are indistinguishable from those constituting the external laser field (traveling along the z axis). However, our calculations of the tadpole contribution are supposed to examine the accuracy of the LCFA and to survey its justification, which is now possible since Eqs. (8) and (9) relate to the same physical quantity.

Finally, we note that the leading-order contribution corresponding to the diagram with four external legs (see Fig. 2) could contain gauge-dependent (spurious) terms. In atomic physics, where the Coulomb potential of the nucleus is conventionally described by means of the scalar component A^0 of the electromagnetic potential, it is a well-elaborated issue. It was demonstrated (see Refs. [31–34]) that Pauli-Villars regularization [35] reveals a nontrivial contribution even when the electron mass tends to infinity. This term is gauge-dependent and should be subtracted from the diagram. Nevertheless, in the gauge (1) there is no spurious term (the proof can be found in Supplemental Material [28]), which was also confirmed by our numerical computations.

As the vertex contribution does not require renormalization, it can be evaluated by means of Eq. (3), which in the case of a

standing wave yields

$$\frac{(2\pi)^3}{V} n_{\mathbf{k},\lambda}^{(\text{vertex})} = \frac{e^2}{(2\pi)^3} \frac{1}{2k^0} \sum_{s,s'} \int d\mathbf{p} \times \left| \sum_{j,l} \int dt {}_+ \bar{w}_{-\mathbf{p},s}^j(t) \gamma^\mu \varepsilon_\mu^*(\mathbf{k}, \lambda) - {}_+ w_{\mathbf{p}-\mathbf{k}-l\mathbf{K},s'}^{l-j}(t) e^{ik^0 t} \right|^2$$

When integrating over $t \in (-\infty, t_{\text{in}}]$ and $t \in [t_{\text{out}}, +\infty)$, one should introduce a standard factor $e^{-\varepsilon|t|}$ ($\varepsilon \rightarrow 0$) and calculate the integral over these rays analytically (see Ref. [27] for more detail). Note that a crucial difference between the tadpole and vertex contributions lies in the conservation laws. Whereas the tadpole term describes the process of photon production by absorption/emission of the external-field photons, the vertex diagram contains also e^+e^- pair whose energy can continuously vary. It explains why in the former case the signal photons tend to have the same quantum numbers as the external-background photons (e.g., $k^0 \approx \omega$), while in the latter case they are likely to have a very small energy, $k^0 \ll \omega$, no matter which external-field configuration is chosen. It means first that these two contributions can be analyzed separately. Second, since for a spatially uniform field, Eq. (10) becomes much less complicated and the momentum conservation law does not appear to play a vital role here, it seems sensible to perform the calculations replacing the external field (1) with a time-dependent background corresponding to a given position z and to average the results over the spatial period of the standing wave. We will also refer to this approximate technique as the LCFA, and its predictions will be benchmarked

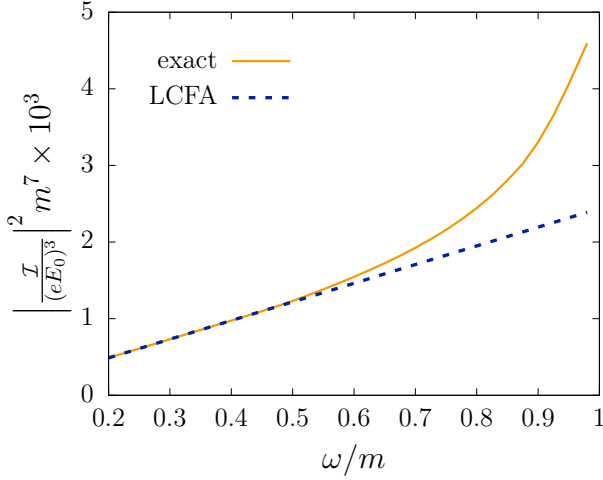


Figure 3. Leading-order contribution to the tadpole diagram evaluated by means of Eq. (8) (exact) and Eq. (9) (LCFA) as a function of ω .

against those obtained by means of the exact expression (10). As was demonstrated in Ref. [27], for small values of k^0 , the integral over $t \in [t_{\text{out}}, +\infty)$ in Eq. (10) scales as $1/k^0$, which leads to

$$\frac{(2\pi)^3}{V} n_{\mathbf{k},\lambda}^{(\text{vertex})} = \frac{e^2}{(2\pi)^3} \frac{C_\lambda}{(k^0)^3} + \mathcal{O}\left(\frac{1}{(k^0)^2}\right) \quad (11)$$

for $k^0 \rightarrow 0$. Our calculations proved this asymptotic behavior to remain valid also in the presence of spatial inhomogeneities. In what follows, we will compare the exact results with the LCFA predictions in terms of the coefficient $C = \sum_\lambda C_\lambda$ depending on E_0 , ω , and the direction of \mathbf{k} . Since $d\mathbf{k} = k_0^2 d\Omega dk_0$, the coefficient C represents the energy density of photons emitted, which turns out to be almost independent of k_0 , provided k_0 is sufficiently small.

To perform exact calculations in the case of a standing wave, we numerically evolve the necessary Fourier components $\zeta w_{p,s}^j(t)$ and evaluate then the expression (10). Our numerical procedures propagating solutions of the Dirac equation were already successfully employed in several studies concerning e^+e^- pair production [19, 20, 26, 30, 36]. To make sure that we receive reliable data, we first reproduced the results of Otto and Kämpfer [27] and conducted our computations in two different coordinate systems, i.e., we employed Eq. (1) and a similar expression with the substitution $x \leftrightarrow z$.

Numerical results.—In Fig. 3 we draw a comparison between the exact results and the LCFA predictions for the leading-order contribution to the tadpole diagram in terms of $|Z|^2$ [see Eqs. (8) and (9)] for various values of the carrier frequency ω . The factor $m^6/(eE_0)^3$ is introduced to make the results independent of E_0 . We observe that for $(\omega/m)^2 \lesssim 0.3$ the LCFA accurately reproduces the exact results, whereas for larger values of ω it considerably underestimates the photon yield. Although the condition $(\omega/m)^2 \ll 1$ justifying the LCFA was already discussed in the literature (see, e.g.,

Ref. [37]), the deviation between the LCFA predictions and the exact results was unknown as the latter data has been unavailable until now.

With regard to the vertex contribution, we first underline the fact that the asymptotic behavior (11) holds even if one performs the exact computations according to Eq. (10). Note also that within the LCFA the y and z axes are completely equivalent, while beyond this approximation all of the three spatial directions are different due to the presence of the magnetic field component. The corresponding C coefficients will be denoted by C_x , C_y , and C_z , e.g., C_x relates to $\mathbf{k} = (k^0, 0, 0)$ in Eq. (11). Within the LCFA we have $C_x = C_\parallel$ and $C_y = C_z = C_\perp$.

In Fig. 4 we display the dependence $C(E_0)$ computed exactly and within the LCFA. Concerning the approximate treatment, the plot (solid and dashed lines) reveals two important features. First, one can easily establish the scaling law $C(E_0) \sim E_0^2$ for sufficiently small E_0 . Our calculations for other values of ω demonstrated that the corresponding threshold value of E_0 increases with decreasing ω , so the Keldysh parameter $\gamma = m\omega/|eE_0|$ decreases, e.g., for $\omega = 0.5m$ it amounts to $\gamma = 1.2$, whereas for $\omega = 0.25m$ it is $\gamma = 0.44$. It means that for $\omega \lesssim 0.1m$ the scaling law is always valid once the pair-production process, which accompanies photon emission in the vertex diagram, reflects nonperturbative nature, $\gamma \lesssim 1$. Second, the function $C(E_0)$ becomes independent of the direction of the photons emitted, i.e. $C_\parallel \approx C_\perp$. Accordingly, the LCFA predicts a great number of soft photons that are emitted isotropically and whose energy density is proportional to E_0^2 as long as γ is comparable to or larger than unity.

The results obtained beyond the LCFA are depicted in Fig. 4 for each of the three spatial directions. The scaling law $C(E_0) \sim E_0^2$ remains valid, but the emission process is no longer isotropic. Although the curve corresponding to the magnetic field direction y almost coincides with that of $C_\parallel(E_0) \approx C_\perp(E_0)$, for the x and z axes the results are different. While in the former case the coefficient $mC/|eE_0|^2$ amounts to 3×10^{-6} , in the latter case it is two times larger, 6×10^{-6} . These quantitative characteristics predict a notable anisotropy which is expected to be observable in experiment providing a distinctive feature which is not described by the LCFA. The findings discussed above were also confirmed by our computations with other values of ω .

Conclusions.—We performed exact calculations of both the tadpole and vertex contributions to the number density of photons emitted in the presence of a standing electromagnetic wave. By rigorously treating the temporal and spatial inhomogeneities, we made a first step beyond the previously-used approximation. In particular, the results obtained for the tadpole diagram uncovered a substantial underestimation of the photon yield which takes place within the LCFA for sufficiently high frequency of the external field. Concerning the vertex contribution, the exact computations predict a large amount of soft photons whose energy density is proportional to E_0^2 . More important, the additional radiation is, in fact, anisotropic in contrast to the LCFA results: the number of photons emitted along the y direction is twice as small as the analogous quan-

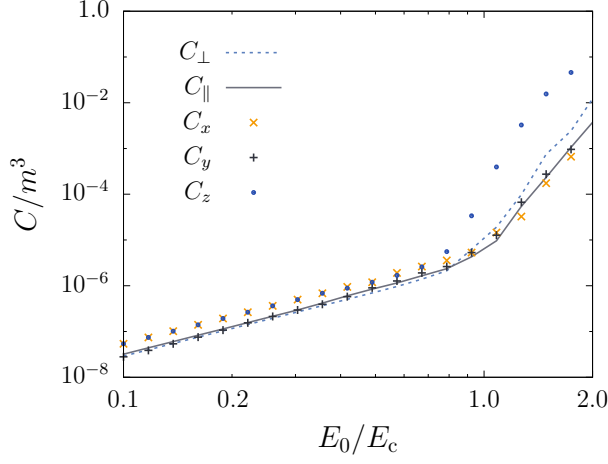


Figure 4. Exact values of the C coefficients corresponding to the three spatial directions x , y , and z and the LCFA results for C_{\parallel} and C_{\perp} as a function of E_0 ($\omega/m = 0.25$).

tity regarding the x and z axes. This fact represents a new important signature which can allow one not only to advance the experimental studies of this phenomenon but also to validate more accurate theoretical approaches going beyond the LCFA. We also emphasize that this finding holds true once $\gamma \lesssim 1$, which corresponds to the nonperturbative domain of pair production where detection of photons may open up a possibility of indirect experimental observation of the Schwinger effect. Our results are expected to significantly broaden our understanding of nonlinear QED effects supporting further improvement of our knowledge and of the necessary theoretical techniques in pursuit of practical investigations of strong-field QED phenomena.

This work was supported by Russian Foundation for Basic Research (RFBR) and Deutsche Forschungsgemeinschaft (DFG) (Grants No. 17-52-12049 and No. PL 254/10-1) and by Saint Petersburg State University (SPbSU) and DFG (Grants No. 11.65.41.2017 and No. STO 346/5-1). I.A.A. also acknowledges the support from the FAIR-Russia Research Center and from the Foundation for the advancement of theoretical physics and mathematics BASIS.

APPENDIX: GENERAL EXPRESSIONS FOR THE PHOTON NUMBER DENSITY

Here we will present a short derivation of Eqs. (2) and (3) from the main text of the Letter, i.e., we will evaluate the photon number density to first order in α . To this end, we turn to the interaction picture taking into account the interaction operator $H_{\text{int}} = j_{\mu}(x)\hat{A}^{\mu}(x)$ within PT. Here $j_{\mu}(x)$ is the current operator of the electron-positron field, and $\hat{A}^{\mu}(x)$ is the quantized part of the electromagnetic field. The corresponding S

operator reads

$$S = T \exp \left(-i \int_{t_{\text{in}}}^{t_{\text{out}}} H_{\text{int}}(t) dt \right) \quad (\text{A1})$$

and has the following PT series $[S = S^{(0)} + S^{(1)} + \dots]$:

$$S^{(0)} = 1, \quad (\text{A2})$$

$$S^{(1)} = -i \int_{t_{\text{in}}}^{t_{\text{out}}} dt H_{\text{int}}(t), \quad (\text{A3})$$

$$S^{(2)} = \frac{(-i)^2}{2} \int_{t_{\text{in}}}^{t_{\text{out}}} dt_1 \int_{t_{\text{in}}}^{t_{\text{out}}} dt_2 T [H_{\text{int}}(t_1) H_{\text{int}}(t_2)], \quad (\text{A4})$$

...

The quantized part of the electromagnetic field is decomposed according to

$$A_{\mu}(x) = \sum_{\lambda=0}^3 \int d\mathbf{k} \left[c_{\mathbf{k},\lambda} f_{\mathbf{k},\lambda,\mu}(x) + c_{\mathbf{k},\lambda}^{\dagger} f_{\mathbf{k},\lambda,\mu}^*(x) \right], \quad (\text{A5})$$

where $c_{\mathbf{k},\lambda}^{\dagger}$ and $c_{\mathbf{k},\lambda}$ are the photon creation and annihilation operators, respectively. In what follows, we will also need the following expansion of the electron-positron field operator in terms of the *in* one-particle solutions of the Dirac equation:

$$\psi(x) = \sum_n [a_n + \varphi_n(x) + b_n^{\dagger} - \varphi_n(x)], \quad (\text{A6})$$

where we have introduced the electron (positron) creation and annihilation operators a_n^{\dagger} (b_n^{\dagger}) and a_n (b_n), respectively. These operators satisfy the usual anticommutation relations.

In Ref. [15] the authors evaluated transition amplitudes, i.e., S -matrix elements, describing the process of photon emission from the vacuum state in the presence of a strong classical external field. Although the corresponding expressions give essentially the leading-order contributions to the photon number density, we will present here an alternative approach based on direct calculation of the mean value of the photon number operator. The exact expression for this quantity reads

$$n_{\mathbf{k},\lambda} = \langle 0, \text{in} | S^{\dagger} c_{\mathbf{k},\lambda}^{\dagger} c_{\mathbf{k},\lambda} S | 0, \text{in} \rangle. \quad (\text{A7})$$

To zeroth order, the field does not generate any photons. Since the interaction Hamiltonian contains terms with only one photon creation/annihilation operator, it is clear that the first-order contribution to the number density (A7) also vanishes. So the main task is to calculate the second-order term given by

$$n_{\mathbf{k},\lambda}^{(2)} = \langle 0, \text{in} | S^{(1)\dagger} c_{\mathbf{k},\lambda}^{\dagger} c_{\mathbf{k},\lambda} S^{(1)} | 0, \text{in} \rangle. \quad (\text{A8})$$

In order to perform these calculations, one should express the current operator $j^{\mu}(x) = (e/2)[\bar{\psi}(x)\gamma^{\mu}, \psi(x)]$ in terms of the *in* operators. This can be done by means of Eq. (A6),

so one receives

$$j^\mu(x) = e \sum_{l,s} [(+\bar{\varphi}_l \gamma^\mu + \varphi_s) a_l^\dagger a_s + (+\bar{\varphi}_l \gamma^\mu - \varphi_s) a_l^\dagger b_s^\dagger - (-\bar{\varphi}_s \gamma^\mu + \varphi_l) a_l b_s - (-\bar{\varphi}_s \gamma^\mu - \varphi_l) b_l^\dagger b_s] + \frac{e}{2} \sum_l [(-\bar{\varphi}_l \gamma^\mu - \varphi_l) - (+\bar{\varphi}_l \gamma^\mu + \varphi_l)], \quad (\text{A9})$$

where the one-particle functions depend on x . The term displayed in the third line of Eq. (A9) represents the *in*-vacuum

expectation value $j_{\text{in}}^\mu(x) \equiv \langle 0, \text{in} | j^\mu(x) | 0, \text{in} \rangle$ (vacuum current). The corresponding contribution will be referred to as the tadpole (reducible) one, while the rest part of $j^\mu(x)$ in Eq. (A9) will give rise to the vertex (irreducible) term. After some straightforward calculations, one obtains

$$n_{\mathbf{k},\lambda}^{(2)} = n_{\mathbf{k},\lambda}^{(\text{tadpole})} + n_{\mathbf{k},\lambda}^{(\text{vertex})}, \quad (\text{A10})$$

where

$$n_{\mathbf{k},\lambda}^{(\text{tadpole})} = \left| \int d^4x j_{\text{in}}^\mu(x) f_{\mathbf{k},\lambda,\mu}^*(x) \right|^2 = \frac{e^2}{4} \left| \sum_n \int d^4x [+\bar{\varphi}_n(x) \gamma^\mu + \varphi_n(x) - -\bar{\varphi}_n(x) \gamma^\mu - \varphi_n(x)] f_{\mathbf{k},\lambda,\mu}^*(x) \right|^2, \quad (\text{A11})$$

$$n_{\mathbf{k},\lambda}^{(\text{vertex})} = e^2 \sum_{n,m} \left| \int d^4x +\bar{\varphi}_n(x) \gamma^\mu f_{\mathbf{k},\lambda,\mu}^*(x) - \varphi_m(x) \right|^2. \quad (\text{A12})$$

The expressions (A11) and (A12) coincide with (2) and (3).

APPENDIX: SPURIOUS TERMS OF THE TADPOLE DIAGRAM

As was indicated in the main text, the diagram containing four vertices (see Fig. 5) could lead to gauge-dependent contributions which should be subtracted. A recipe for extracting these spurious terms is based on the Pauli-Villars regularization procedure [35]. One should replace the electron mass with some mass M and evaluate the diagram assuming $M \rightarrow \infty$ [31–34]. The photon wave function correspond-

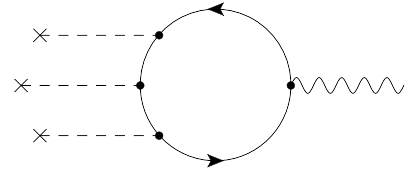


Figure 5. Feynman diagram providing a leading-order term of the tadpole contribution. The solid (fermionic) lines correspond now to the electron propagator involving large mass M .

ing to the external photon line in Fig. 5 is contracted with the current operator $j_{\text{in}}^{(3)\mu}(x)$ which has the following form:

$$j_{\text{in}}^{(3)\mu}(x) = -ie^4 \int dz_1 \int dz_2 \int dz_3 \text{Tr} [\gamma^\mu S_M(x, z_1) \gamma^\nu A_\nu(z_1) S_M(z_1, z_2) \gamma^\rho A_\rho(z_2) S_M(z_2, z_3) \gamma^\sigma A_\sigma(z_3) S_M(z_3, x)], \quad (\text{A13})$$

where the subscript M indicates that the propagators contain now large mass M . Since $M \rightarrow \infty$, the integrals in (A13) receive nonzero contributions only from the vicinity of $z_1 = z_2 = z_3 = x$, which allows one to replace the arguments of A with x . We will also employ the following representation:

$$S_M(x, y) = \int_{C_F} \frac{d\omega}{2\pi} e^{-i\omega(x^0 - y^0)} g(\mathbf{x}, \mathbf{y}, \omega), \quad (\text{A14})$$

where C_F denotes the usual contour corresponding to the Feynman propagator,

$$g(\mathbf{x}, \mathbf{y}, \omega) = \int \frac{d\mathbf{p}}{(2\pi)^3} e^{i\mathbf{p}(\mathbf{x}-\mathbf{y})} \frac{\omega \gamma^0 - \boldsymbol{\gamma} \mathbf{p} + M}{p_0^2 - \omega^2}, \quad (\text{A15})$$

and $p_0 = \sqrt{M^2 + \mathbf{p}^2}$. Using Eqs. (A14) and (A15) and integrating over z_i in Eq. (A13), one obtains

$$j_{\text{in}}^{(3)\mu}(x) = -ie^4 A_\nu(x) A_\rho(x) A_\sigma(x) \int \frac{d\omega}{2\pi} \int \frac{d\mathbf{p}}{(2\pi)^3} \frac{1}{(p_0^2 - \omega^2)^4} \text{Tr} [\gamma^\mu \Gamma(\mathbf{p}, \omega) \gamma^\nu \Gamma(\mathbf{p}, \omega) \gamma^\rho \Gamma(\mathbf{p}, \omega) \gamma^\sigma \Gamma(\mathbf{p}, \omega)], \quad (\text{A16})$$

where $\Gamma(\mathbf{p}, \omega) \equiv \omega \gamma^0 - \boldsymbol{\gamma} \mathbf{p} + M$. In the case of a nontrivial scalar potential ($A_0 \neq 0$, $\mathbf{A} = 0$), this expression yields

$$j_{\text{in}}^{(3)0}(x) = -\frac{e^4 A_0^3(x)}{3\pi^2} \quad (\text{A17})$$

in accordance with Refs. [31–34].

If we assume that A^μ has one nontrivial spatial component, e.g., $A_0 = A_x = A_y = 0$ and $A_z \neq 0$, then the trace in Eq. (A16) gives us odd functions of p_z for each $\mu = 0, 1, 2$. Accordingly, integration over p_z yields zero. For $\mu = 3$, one obtains $\text{Tr}[\dots] = 4(p_z^4 - 6ap_z^2 + a^2)$, where $a \equiv M^2 + p_x^2 +$

$p_y^2 - \omega^2$. In this case, the integral over p_z also vanishes:

$$\int_{-\infty}^{+\infty} dp_z \frac{p_z^4 - 6ap_z^2 + a^2}{(a + p_z^2)^4} = 0. \quad (\text{A18})$$

Therefore, there is no spurious contribution for the field configuration and gauge chosen.

-
- [1] H. Euler and B. Kockel, *Naturwissenschaften* **23**, 246 (1935)
 - [2] W. Heisenberg and H. Euler, *Z. Phys.* **98**, 714 (1936).
 - [3] V. Weisskopf, *Kong. Dans. Vid. Selsk., Mat.-fys. Medd.* **XIV**, 6 (1936).
 - [4] J. Schwinger, *Phys. Rev.* **82**, 664 (1951).
 - [5] R. Karplus and M. Neuman, *Phys. Rev.* **80**, 380 (1950); **83**, 776 (1951).
 - [6] H. Gies, F. Karbstein, and C. Kohlfürst, *Phys. Rev. D* **97**, 036022 (2018).
 - [7] H. Gies, F. Karbstein, C. Kohlfürst, and N. Seegert, *Phys. Rev. D* **97**, 076002 (2018).
 - [8] A. Blinne, H. Gies, F. Karbstein, C. Kohlfürst, and M. Zepf, *Phys. Rev. D* **99**, 016006 (2019).
 - [9] F. Karbstein, A. Blinne, H. Gies, and M. Zepf, *Phys. Rev. Lett.* **123**, 091802 (2019).
 - [10] A. Di Piazza, K. Z. Hatsagortsyan, and C. H. Keitel, *Phys. Rev. D* **72**, 085005 (2005).
 - [11] A. M. Fedotov and N. B. Narozhny, *Phys. Lett. A* **362**, 1 (2006).
 - [12] N. B. Narozhny and A. M. Fedotov, *Laser Phys.* **17**, 350 (2007).
 - [13] B. King, H. Hu, and B. Shen, *Phys. Rev. A* **98**, 023817 (2018).
 - [14] H. Gies and F. Karbstein, *J. High Energy Phys.* **03** (2017) 108.
 - [15] E. S. Fradkin, D. M. Gitman, and S. M. Shvartsman, *Quantum Electrodynamics with Unstable Vacuum* (Springer-Verlag, Berlin, 1991).
 - [16] A. Di Piazza, M. Tamburini, S. Meuren, and C. H. Keitel, *Phys. Rev. A* **98**, 012134 (2018).
 - [17] T. G. Blackburn, D. Seipt, S. S. Bulanov, and M. Marklund, *Phys. Plasmas* **25**, 083108 (2018).
 - [18] A. Ilderton, B. King, and D. Seipt, *Phys. Rev. A* **99**, 042121 (2019).
 - [19] I. A. Aleksandrov, G. Plunien, and V. M. Shabaev, *Phys. Rev. D* **96**, 076006 (2017).
 - [20] I. A. Aleksandrov, G. Plunien, and V. M. Shabaev, *Phys. Rev. D* **97**, 116001 (2018).
 - [21] C. Kohlfürst and R. Alkofer, *Phys. Rev. D* **97**, 036026 (2018).
 - [22] C. Kohlfürst, *Eur. Phys. J. Plus* **133**, 191 (2018).
 - [23] Q. Z. Lv, S. Dong, Y. T. Li, Z. M. Sheng, Q. Su, and R. Grobe, *Phys. Rev. A* **97**, 022515 (2018).
 - [24] Z. Peng, H. Hu, and J. Yuan, *arXiv:1810.03606*.
 - [25] G. Torgrimsson, C. Schneider, and R. Schützhold, *Phys. Rev. D* **97**, 096004 (2018).
 - [26] I. A. Aleksandrov, G. Plunien, and V. M. Shabaev, *Phys. Rev. D* **99**, 016020 (2019).
 - [27] A. Otto and B. Kämpfer, *Phys. Rev. D* **95**, 125007 (2017).
 - [28] See Supplemental Material at [URL will be inserted by publisher] for the derivation of the expressions (2) and (3) and for the proof of the absence of the spurious contribution to the diagram with four external legs.
 - [29] A. Wöller, H. Bauke, and C. H. Keitel, *Phys. Rev. D* **91**, 125026 (2015).
 - [30] I. A. Aleksandrov, G. Plunien, and V. M. Shabaev, *Phys. Rev. D* **94**, 065024 (2016).
 - [31] M. Gyulassy, *Nucl. Phys. A* **244**, 497 (1975).
 - [32] G. A. Rinker and L. Wilets, *Phys. Rev. A* **12**, 748 (1975).
 - [33] E. Borie and G. A. Rinker, *Rev. Mod. Phys.* **54**, 67 (1982).
 - [34] G. Soff and P. J. Mohr, *Phys. Rev. A* **38**, 5066 (1988).
 - [35] W. Pauli and F. Villars, *Rev. Mod. Phys.* **21**, 434 (1949).
 - [36] I. A. Aleksandrov, G. Plunien, and V. M. Shabaev, *Phys. Rev. D* **95**, 056013 (2017).
 - [37] F. Karbstein and R. Shaisultanov, *Phys. Rev. D* **91**, 085027 (2015).